Alumina-SiC composites for enhanced ballistic performance using Spark Plasma Sintering

Guillaume Rayrat, Yann Bald, Florence Moitrier, Paul Beillard, Anthony Bracq, Sébastien Lemonnier, Frédéric Bernard, Sylvain Marinel, Fabian Delorme

Alumina-SiC composites for enhanced ballistic performance using Spark Plasma Sintering

Guillaume Rayrat[1,2,3], Yann Bald[1], Florence Moitrier[1], Paul Beillard[1], Anthony Bracq[1], Sébastien Lemonnier[1], Frédéric Bernard[2], Sylvain Marinel[3], Fabian Delorme[1]

[1]French-German Research Institute of Saint-Louis, 5 rue du Général Cassagnou, BP 70034, 68301, Saint Louis CEDEX, France
[2]ICB - UMR, 6303 Université Bourgogne Europe / CNRS, 9, Av. A. Savary BP 47870, 21078, Dijon, Cedex, France
[3]Université de Normandie, ENSICAEN, UNICAEN, CNRS, CRISMAT, 14000, Caen, France

Keywords: Spark Plasma Sintering, mechanical properties, armor, composite, alumina

ABSTRACT

This study explores the influence of SiC reinforcement on the microstructure, mechanical properties and ballistic performance of Al_2O_3-SiC composites fabricated by Spark Plasma Sintering. Composites containing 1 to 30 vol.% SiC were processed using optimized SPS cycles to ensure high densification and controlled microstructural development. The addition of SiC led to significant improvements in hardness, fracture toughness and Young's modulus with the best compromise observed at 25 vol.% SiC, sintered at 1600 °C. At this composition, a 30% reduction in residual depth of penetration versus 7.62 mm×51 FMJ/PB/HC AP P80 (.308 Win) threat was measured compared to pure alumina, confirming the effectiveness of SiC reinforcement in enhancing ballistic resistance. Although higher SiC contents (≥25 vol.%) resulted in the formation of mullite and a slight decrease in fracture toughness, the 25 vol.% SiC composite offers an optimal balance between mechanical performance and cost-efficiency. These results position Al_2O_3-SiC composites as promising materials for lightweight and affordable ballistic protection systems.

I. INTRODUCTION

Ceramics are widely recognized for their potential in ballistic applications due to their high mechanical properties and low density, which offer an outstanding strength-to-weight ratio compared to other materials used for the same purpose [1,2]. Among them, silicon carbide (SiC) and boron carbide (B_4C) are particularly valued for their exceptional ballistic performances, attributed to their high hardness and low density [3,4]. However, the high production costs of these advanced ceramics limit their widespread use, especially in applications where large-scale deployment and cost control are critical.

Alumina (Al_2O_3), by contrast, stands out for its attractive balance between cost and performance, making it one of the preferred ceramics for ballistic applications [5,6]. This is especially relevant in defense and security contexts, where there is a growing demand for affordable armor systems that provide high protection levels while maintaining operational effectiveness and scalability. The effectiveness of ballistic ceramics depends on multiple factors, including damage resistance, energy absorption capability and behavior under multi-hit conditions [7,8].

To enhance the mechanical properties of alumina while maintaining its cost-effectiveness, recent research has focused on the development of composite materials incorporating a secondary phase [9,10]. In particular, alumina reinforced with SiC particles has emerged as a promising approach, combining the cost benefits of alumina with the superior mechanical properties of SiC. The addition of SiC was found to significantly improve the flexural strength of alumina (up to ~1 GPa for composites versus 350 MPa for pure alumina) as well as the fracture toughness, hardness and wear resistance [11–14]. Furthermore, the lower density of SiC (3.21 $g.cm^{-3}$) contributes to reducing the overall mass of the composite, an essential criterion for lightweight armor systems [15].

The reinforcement mechanisms provided by SiC have been extensively documented. During sintering, SiC particles inhibit grain growth in the alumina matrix [16,17], resulting in a refined microstructure with improved mechanical properties. At the same time, they tend to slow down alumina densification, requiring higher sintering temperatures as the SiC content increases [18–20]. Beyond microstructural refinement, SiC also activates several extrinsic toughening mechanisms such as crack deflection, microcracking, and crack branching [18,21], arising from the mismatch in thermal expansion coefficients (Al_2O_3: $8.1\times10^{-6}.K^{-1}$, SiC: $4.0\times10^{-6}.K^{-1}$) and elastic moduli (Al_2O_3: 350-400 GPa, SiC: 400-460 GPa) [22–24]. This mismatch generates localized residual stresses during cooling, which are tensile in the alumina matrix and compressive within SiC particles. Several studies [25–27] have shown that these stresses can induce the formation and motion of dislocations in alumina, thereby relaxing intrinsic tensile stresses and enlarging the crack-tip process zone. This residual-stress-assisted mechanism complements crack deflection and bridging at Al_2O_3-SiC interfaces, enhancing both strength and fracture toughness. In addition, SiC strengthens grain boundaries and promotes a transition from intergranular to mixed intergranular-transgranular fracture modes, increasing energy absorption during crack propagation [28]. However, when the SiC content is excessive or the second phase is coarsely dispersed, residual stresses may instead promote interfacial decohesion or microcracking, which can counteract these benefits [29]. Altogether, these combined mechanisms make Al_2O_3-SiC composites highly attractive for applications requiring improved mechanical performance and superior energy absorption.

While the mechanical improvements provided by SiC reinforcement are well documented, their direct translation into ballistic performance remains unclear. Most existing studies have either focused on mechanical characterization or employed numerical simulations to predict ballistic behavior, with limited experimental validation of these models. For instance, Azarafza et al. [30] demonstrated through simulations that incorporating 10 vol.% SiC into alumina significantly enhances ballistic performance, reducing back layer

dishing by more than 50%, from 5 mm (pure alumina) to 2 mm. This improvement was attributed to the superior flexural strength and fracture toughness of the composite. However, to date, no experimental study has systematically evaluated the influence of SiC addition on the ballistic performance of alumina.

By contrast, recent work on B_4C-SiC composites provides useful insight. Jamale et al. [31] reported that incorporating 10 wt.% SiC into B_4C reduced the residual velocity of WC-Co projectiles by 74% compared to 50% for monolithic B_4C, while also decreasing the depth of penetration. This improvement was associated with enhanced grain boundary cohesion, suppression of B_4C amorphization under high strain, and improved energy absorption during impact. Although such results have not yet been reported for Al_2O_3-based ceramics, the similar fracture mechanisms suggest that SiC reinforcement could also provide significant benefits for alumina, thereby justifying the focus of the present study.

Spark plasma sintering (SPS) is a particularly effective method for fabricating alumina-SiC composites [32,33]. This technique provides precise control over sintering parameters such as temperature, pressure, and holding time. SPS enables the production of highly dense composites (>99% relative density) at lower temperatures (~1500-1600°C) compared to conventional methods [33–35]. By limiting grain growth, SPS further enhances mechanical properties. However, interfacial reactions between alumina and silicon carbide can lead to the formation of silica-rich amorphous phases or mullite ($3A1_2O_3 \cdot 2SiO_2$) [36,37]. These reactions are promoted by oxygen impurities, such as native SiO_2 layers on SiC particles or residual oxygen in the SPS atmosphere. Although the rapid heating rates, short dwell times, and vacuum environment of SPS help limit these reactions, temperatures above ~1550-1700°C can still favor mullite formation [18,35]. Mullite is generally considered to have inferior mechanical properties compared to pure alumina [38], making it essential to avoid its formation, although its precise impact on Al_2O_3-SiC composite properties remains insufficiently studied.

This study addresses these gaps by experimentally determining the ballistic performance of Al_2O_3-SiC composites with 0 to 30 vol.% SiC, and identifying the optimal reinforcement content to maximize protection. While previous work has largely focused on mechanical properties alone, these do not necessarily predict ballistic ranking, making experimental validation critical. The first part of this work focuses on optimizing SPS parameters to achieve high-density, fine-grained microstructures while minimizing secondary phase formation. Mechanical properties, including Young's modulus, fracture toughness, and hardness, are then characterized alongside ballistic performance. The overall objective is to thoroughly investigate the influence of SiC addition on both the mechanical and ballistic behavior of alumina, with the ultimate goal of developing a high-performance, cost-effective ceramic composite for advanced ballistic protection applications.

II. EXPERIMENTAL PROCEDURE

II.1.1. Elaboration

The starting materials used in this study were commercial α-Al_2O_3 powder (BMA15, Baikowski, France) with a purity of 99.99%, an average particle size of 100-150 nm, and a specific surface area of 15 $m^2.g^{-1}$, as well as α-SiC powder (Sintex 15, Saint-Gobain, France) with a median particle size (d_{50}) of 1.0 µm, a specific surface area of 13 $m^2.g^{-1}$, and with a total of 1.2 wt.% of free SiO_x. The mixtures, containing variable SiC volume fractions (1, 2, 5, 10, 15, 20, 25, and 30 vol.%), were dry-mixed using a planetary ball mill operating at 250 rpm for 1 hour. The milling was performed with 10 mm diameter alumina balls and an 80 mL alumina bowl, maintaining a ball-to-powder mass ratio of 5:1. This process should ensure a homogeneous distribution of SiC within the alumina matrix.

Sintering experiments were conducted using an HP D 125 SPS system (FCT Systeme GmbH, Germany) under dynamic vacuum conditions. Graphite foil was placed between the die and the powder, as well as between the punches and the powder. To minimize radiative heat losses, the die was wrapped in graphite felt. Temperature was monitored by an optical pyrometer focused at the bottom of a hole drilled in the upper punch, positioned 4.5 mm above the ceramic sample. The sintering cycle began with heating to 450°C under constant power. From this point, heating continued at a rate of 50°C.min^{-1} up to the target sintering temperature. Simultaneously, a uniaxial pressure of 50-80 MPa was gradually applied between 450°C and 1000°C, then held constant until the end of the dwell time of the sintering temperature. Following the dwell stage, the pressure was released gradually over 5 minutes during natural cooling.

An initial study was carried out on 30 mm diameter and 4 mm thick samples to determine the sintering temperature range suitable for Al_2O_3-SiC composites and to assess potential reactivity between alumina and SiC. For this preliminary evaluation, all compositions were sintered at 1800°C without a dwell time. Subsequently, a second study was conducted to optimize sintering parameters for each composition before fabricating the targets for ballistic testing. This optimization was performed on 60 mm diameter samples and the thickness was adjusted to ensure a constant areal density of 9 kg.m^{-2} across all compositions, as required for ballistic evaluations. The final sintering temperature varied between 1250°C and 1650°C depending on the SiC content, with a fixed dwell time of 10 min. To determine the potential performance gain associated with the addition of SiC, pure alumina was sintered using the following conditions, determined through prior optimization of the sintering parameters: a reduced heating rate of 25°C.min^{-1} and a shorter dwell time of 3 min. For all the compositions studied, the target of optimization consisted in obtaining a relative density ≥ 99% and a fine microstructure to improve mechanical and ballistic performance.

II.1.2. Characterization

The relative density was determined using Archimedes water displacement method after surface polishing and the theoretical density was considered as 3.987 g.cm^{-3} for alumina (PDF card 00-046-1212) and 3.21 g.cm^{-3} for SiC (PDF card 01-075-8314).

The samples were carefully polished, by standard diamond polishing techniques, down to a diamond particle size of 1 µm, then polished with a 0.05 µm silica slurry with a vibratory polishing machine (Vibromet 2, Buehler, United States). Microstructures were observed on cross sections, using a Field Emission Scanning Electron Microscope (FESEM, FEI NNS 450). The average grain size was estimated from the measurement of several hundred grains on three pictures at the center of each sample with the linear intercept method [39].

The crystalline structure and phase composition of the sintered samples were analyzed using X-ray diffraction (XRD). Diffraction patterns were recorded over a 2θ range of 20 to 80° using a Bruker AXS D8 Advance system (with a step of 0.02° and a counting time of 1 s per step at room temperature) equipped with a copper X-ray tube (CuK_α, $\lambda = 0.15406$ nm). Rietveld refinement was performed using the FullProf software.

The Vickers hardness was measured on polished cross section using a load of 9.8 N and a holding time of 10 s, in accordance with the ASTM C1327 standard [40]. The average hardness value was determined from ten indentations performed at the center of each sample.

The fracture toughness of the samples was evaluated using the Vickers indentation method based on Niihara's model [41]. Indentations were performed with a 19.6 N load and a dwell time of 10 s. The average fracture toughness was determined from ten indentations performed at the center of each sample. Prior to these measurements, a preliminary indentation was conducted to identify the crack morphology, which was

consistently of the Palmqvist type across all samples. The indentation fracture toughness (K_{IC}) was calculated using Equation (1):

$$K_{IC} = 0.0089(\frac{E}{H_V})^{2/5}\frac{P}{a.l^{1/2}} \quad (1)$$

with E the Young's modulus (GPa), H_V the Vickers hardness (GPa), P the applied load during Vickers test (N), l the Palmqvist crack length from the center of the indent to the crack (m) and a the indenter radius (m).

The Young's modulus and Poisson's ratio were determined using the velocities of transverse (V_T) and longitudinal (V_L) ultrasonic waves, measured with an ultrasonic thickness gauge (Olympus 45 MG). From these measurements, the Poisson's ratio (ν) was calculated using Equation (2), and the Young's modulus (E) was determined using Equation (3) [42]:

$$\nu = \frac{1-2(\frac{V_T}{V_L})^2}{2-2(\frac{V_T}{V_L})^2} \quad (2)$$

$$E = \frac{\rho(1+\nu)(1-2\nu)}{(1-\nu)}V_L^2 \quad (3)$$

With ρ the density (kg.m^{-3}) of the sample.

II.1.3. DOP test

The Depth of Penetration (DOP) test was conducted following the configuration described in Fig. 1.

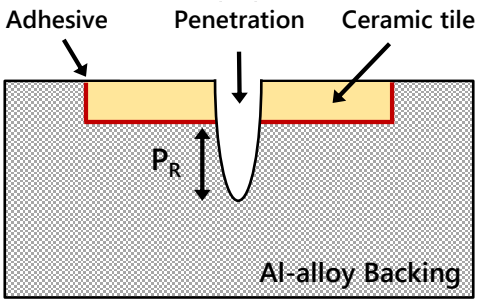

Fig. 1. (a) Schematic illustrating the measurement of residual depth of penetration (P_R), (b) Image showing the aluminum block with a pure alumina target (white) and an Al_2O_3-SiC composite target (grey).

The backing material used in this study is an aluminum alloy (AA7020 T651) with a density of 2.71 g.cm^{-3} and a dimension of 100x100x40 mm^3. Each backing was machined to include a hole with the same dimensions as the ceramic tile (Fig. 2a), which was subsequently bonded into the hole using an adhesive (Permacol 2242 A/B, Fig. 2b). The ballistic tests were conducted on 60 mm diameter targets with an areal density of 9 kg.m^{-2}, with five samples tested for each composition. The projectiles used for this study were 7.62 mm×51 FMJ/PB/HC AP P80 (.308 Win), complying with the VPAM APR 2006 standard [43]. These projectiles were fired at an impact velocity of 820 ± 10 m.s^{-1}.In order to limit the scattering of the data, all the projectiles and aluminum alloy blocks are from the same batch.

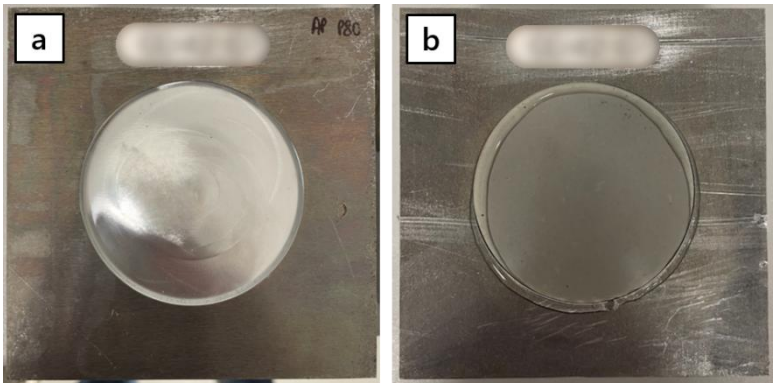

Fig. 2. Preparation of the aluminum block to accommodate the ceramic target (a) and target bonding (b).

Fig. 3a illustrates the experimental setup used for the ballistic tests. The ballistic tests were conducted by first taping the ceramic tile and aluminum alloy backing assembly to a second aluminum block of the same dimensions, which was then securely mounted onto the firing stand (Fig. 3b). Projectiles were fired at the target perpendicularly using a rifled gun positioned 7 meters away.

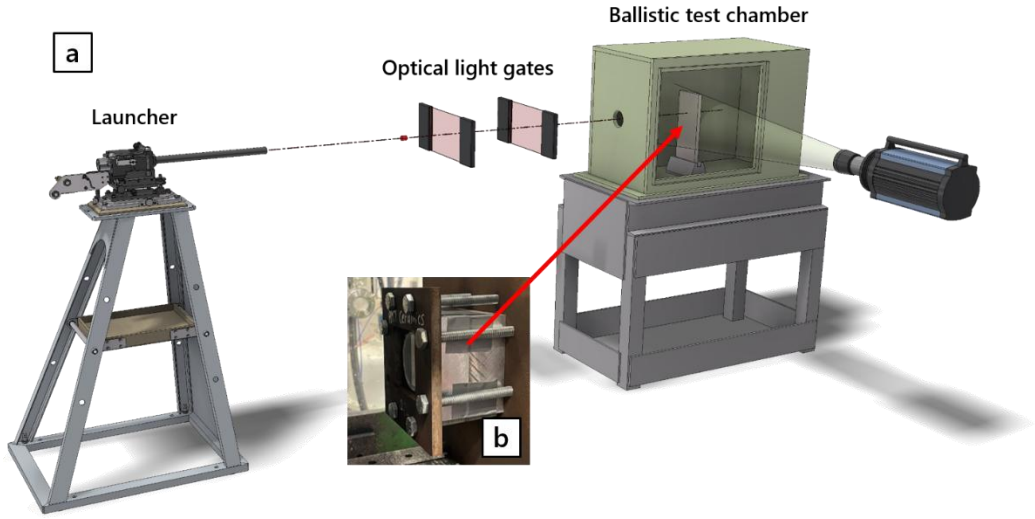

Fig. 3. Simplified schematic of the ballistic test bench (a) and target mounting inside the ballistic test chamber (b).

The velocity and impact angles of the projectiles were recorded with a system combining infrared-emitting diodes and photovoltaic cells, which measures the time intervals between disruptions caused by the projectile passing through two perpendicular beams. These measurements ensure the reliability and validation of the test, with a tolerance of 2° on the impact angle to guarantee its validity. After the ballistic tests, the Al-alloy block was cut in half through the center of the impact (Fig. 4a) to measure the residual depth of penetration (Fig. 4b). The reference penetration depth in the Al-alloy without ceramic is 40.4 mm.

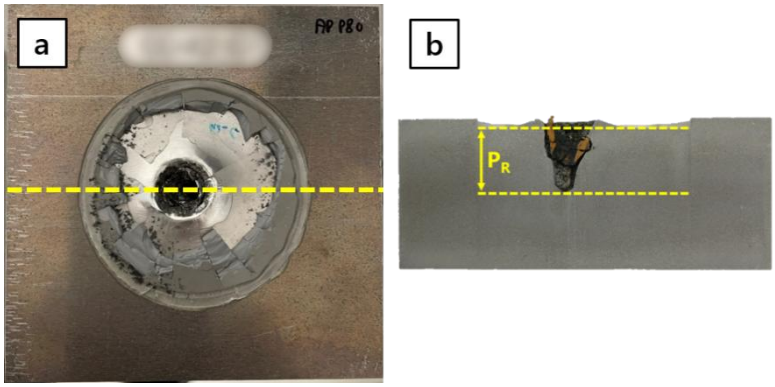

Fig. 4. Post-impact results (a) and residual penetration depth (P_R) measurement after block sectioning (b).

To benchmark the performance of the developed composites as well as the pure alumina samples, additional tests were carried out on commercial silicon carbide (Hexoloy®, Saint-Gobain, France) and alumina (ALOTEC® 99 SB, CeramTec, Germany) ceramics of identical dimensions. These materials are widely used in the production of ballistic protection systems.

III. RESULTS AND DISCUSSION

III.1. Reactivity in the Al_2O_3-SiC system

The initial stage in the development of Al_2O_3-SiC composites consisted in evaluating the reactivity between the two selected phases. To promote the occurrence and detection of potential interfacial reactions, a composite containing 30 vol.% SiC, representing the most reactive configuration within the scope of the study was selected. A preliminary sintering experiment was performed at 1800°C under 50 MPa, a condition sufficient to achieve full densification and to assess the system's reactivity (Fig. 5).

X-ray diffraction analysis of the sample sintered at this temperature revealed the presence of alumina (PDF card 00-046-1212), SiC (PDF card 01-075-8314) and mullite (COD card No. 96-900-1568), the latter identified by its characteristic peaks at 2θ = 16.5° and 26°. A Rietveld refinement performed on the XRD data estimated the mullite content to be approximately 2-3 wt.%. However, this phase could not be clearly distinguished by scanning electron microscopy or EDS mapping, most likely due to its low concentration. Mullite is assumed to form locally at the interface between alumina and surface silica on SiC grains. It may exist as extremely thin layers or develop at grain boundaries, making its detection by SEM particularly challenging.

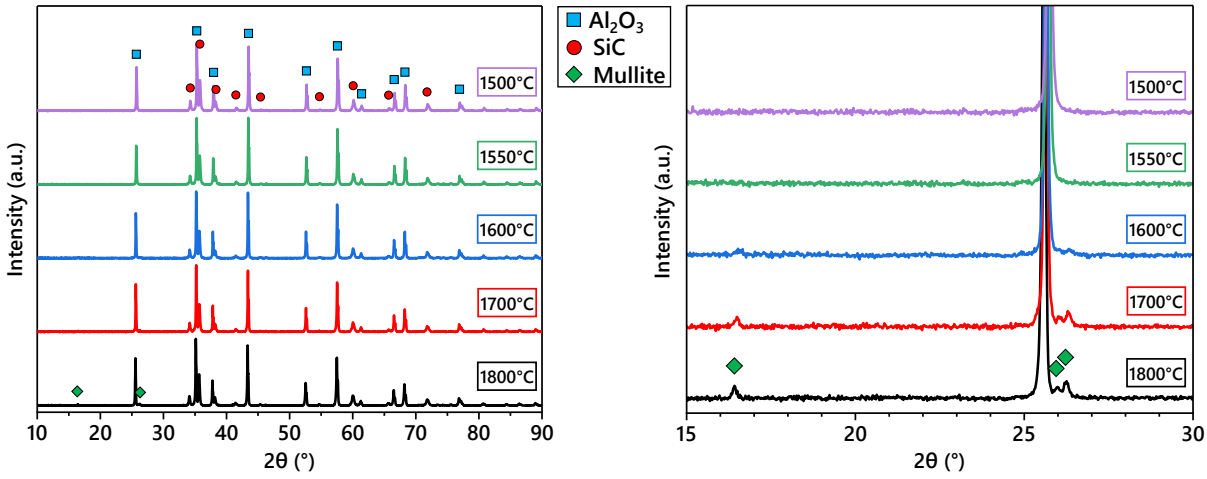

Fig. 5. X-ray diffraction patterns of Al_2O_3-SiC composites containing 30 vol.% SiC, sintered at various temperatures under 50 MPa with no dwell time.

To determine the onset temperature of mullite formation, additional sintering tests were conducted at lower temperatures (Fig. 5). Mullite was detected starting at 1600°C, indicating that its formation begins between 1550 and 1600°C. Therefore, a sintering temperature near 1550°C would be preferable to avoid the formation of mullite, especially if this secondary phase proves detrimental to the ballistic performance of the composite.

The formation of mullite is likely due to the initial oxidation of SiC, promoted by impurities present in the material (1.2 wt.% free SiO_X), which leads to the formation of SiO_2. At temperatures above 1600°C, this silica can then react with alumina to form mullite [18,36] through the following reaction :

$$3\ Al_2O_{3\,(s)} + 2\ SiO_{2\,(s)} \rightarrow 3A1_2O_3{\cdot}2SiO_{2(s)} \qquad (4)$$

The next step of the study will focus on optimizing the sintering parameters, specifically by increasing dwell time and applied pressure, to lower the sintering temperature while ensuring sufficient densification and minimizing the formation of secondary phases such as mullite.

III.2. Optimization of the sintering conditions

III.2.1. Preliminary Study

Optimization of the sintering parameters for Al_2O_3-SiC composites begins with the determination of the temperature required to achieve full densification, regardless of composition. To this end, a series of SPS experiments was carried out at 1800°C under an increased uniaxial pressure of 80 MPa, still without isothermal dwell time. The goal was to determine, for each composition, the temperature at which shrinkage ceases, marking the effective end of densification (Fig. 6).

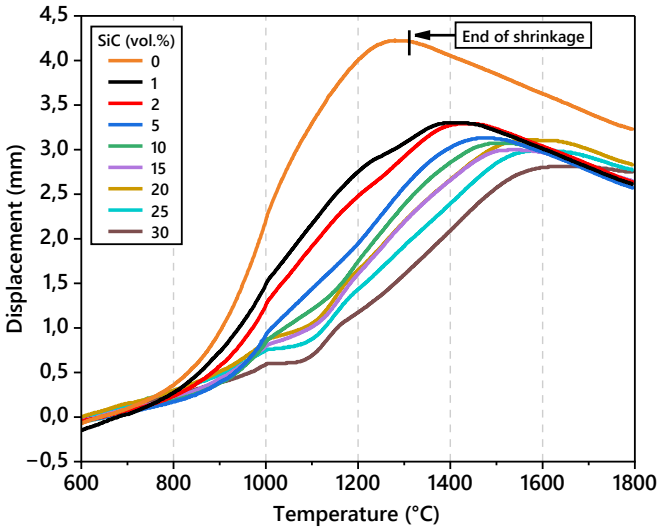

Fig. 6. Effect of SiC content on displacement curves during sintering of Al_2O_3-SiC composites at 1800°C under 80 MPa, without dwell time.

The results show a progressive increase in this final shrinkage temperature with increasing SiC content (Table 1). For example, pure alumina exhibits a final shrinkage temperature of approximately 1290°C, while this value rises to 1650°C for the composite containing 30 vol.% SiC.

Table 1. Final shrinkage temperature, relative density and grain size of Al_2O_3 and Al_2O_3-SiC composites as a function of SiC content after sintering at 1800°C.

SiC content (vol.%)	Final shrinkage temperature (°C)	Relative density (%)	Grain size of alumina (µm)
0	1290	99 ± 1	16.6 ± 0.6
1	1410	99 ± 1	9.1 ± 0.4
2	1440	99 ± 1	7.9 ± 0.4
5	1480	99 ± 1	4.2 ± 0.5
10	1510	99 ± 1	2.9 ± 0.4
15	1540	99 ± 1	1.2 ± 0.2
20	1575	99 ± 1	0.8 ± 0.1
25	1600	99 ± 1	0.7 ± 0.1
30	1650	98 ± 1	0.5 ± 0.1

This trend is attributed to several mechanisms induced by the presence of SiC within the alumina matrix. Firstly, due to its highly refractory nature, SiC does not actively contribute to sintering mechanisms within the temperature range typically used for alumina. Secondly, the incorporation of SiC reduces the number of Al_2O_3 -Al_2O_3 grain contacts, which are essential for efficient diffusion and grain boundary mobility. The increased fraction of Al_2O_3-SiC heterogeneous interfaces leads to higher interfacial energies and lower mass transport efficiency, thereby hindering grain boundary migration and limiting grain growth [44]. Moreover, the potential presence of silica on the surface of SiC particles, either as an impurity or formed by oxidation, can result in the formation of glassy or reactive phases. These secondary phases may locally reduce diffusion coefficients and even promote unwanted reactions, such as the formation of mullite at high temperature.

As a result, above 25 vol.% SiC, the final shrinkage temperature exceeds 1600°C, highlighting the need for careful optimization of sintering parameters to avoid secondary phase formation and ensure microstructural integrity. Despite these challenges, all composites reached a relative density of 99%, except the composition with 30 vol.% SiC, which exhibited a slightly lower final density, around 98%. XRD analysis (Fig. 7) confirmed the formation of mullite in composites containing at least 5 vol.% SiC. Although not detected at lower concentrations, the formation of mullite at these levels remains probable, but likely falls below the detection limit of the technique.

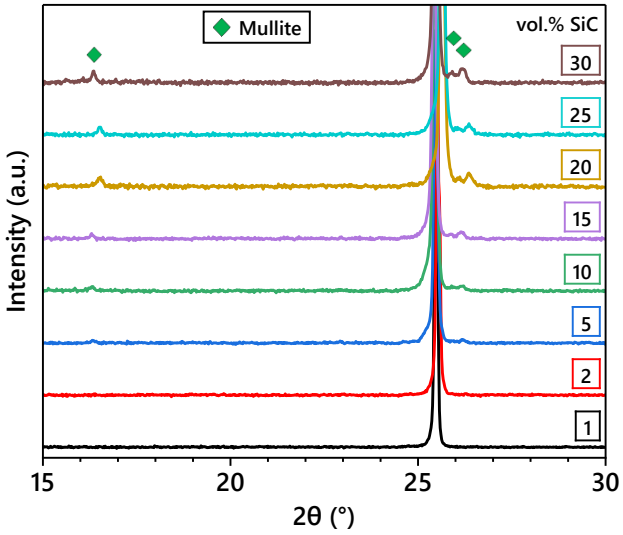

Fig. 7. X-ray diffraction patterns (15–30° range) of Al_2O_3-SiC composites sintered at 1800°C.

Fig. 8 presents the evolution of the microstructure as a function of SiC volume fraction. Under identical sintering conditions (1800°C), a significant refinement of the alumina grain size is observed with increasing SiC content. This refinement is particularly marked at lower SiC fractions: from 16 µm for pure alumina to approximately 1.2 µm for the composite containing 15 vol.% SiC. Beyond this composition, the grain size continues to decrease, though more gradually, reaching about 0.5 µm at 30 vol.% SiC (Table 1). This behavior supports the hypothesis that SiC particles reduce grain boundary mobility, a phenomenon commonly referred to as grain boundary pinning by secondary phases, and already documented in the Al_2O_3-SiC system [45–47]. Microstructural observations further suggest that above 15 vol.% SiC, grain growth is effectively suppressed, resulting in an alumina grain size that closely approaches that of the starting powder.

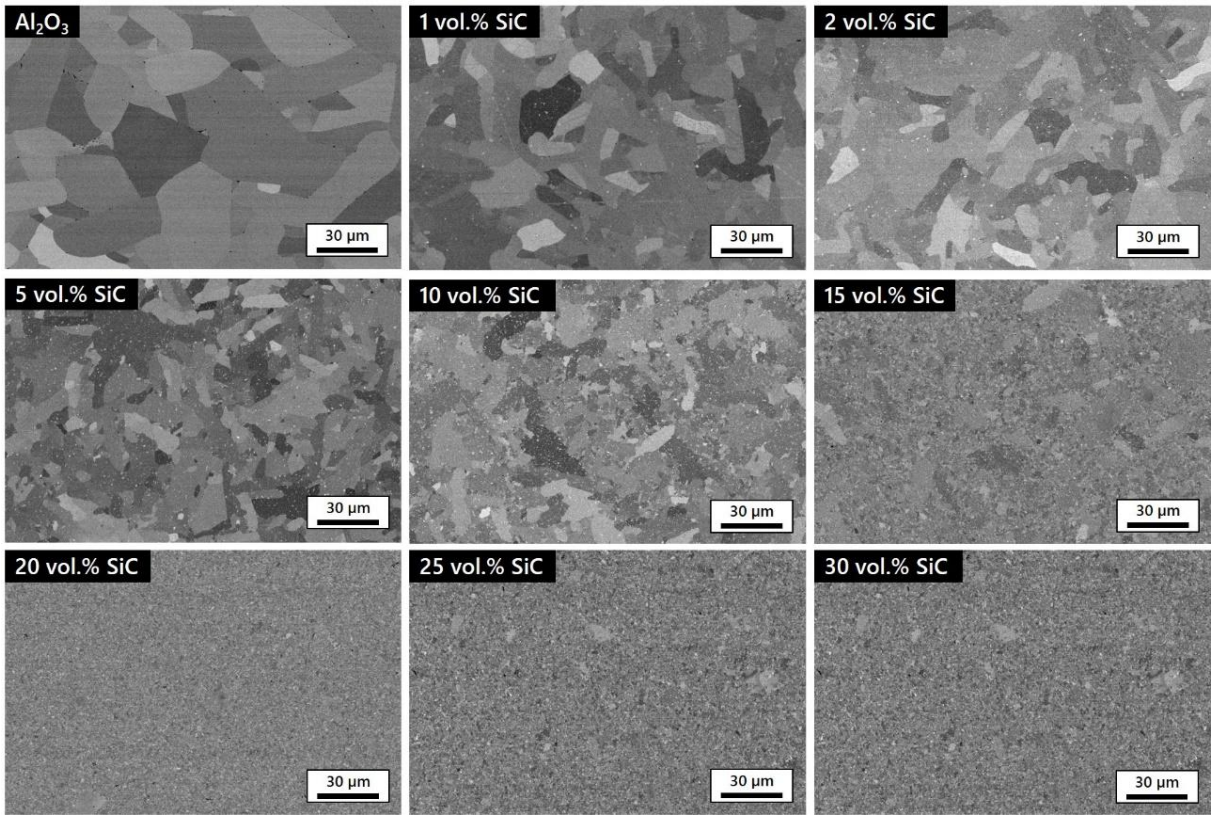

Fig. 8. Microstructures of Al_2O_3-SiC composites sintered at 1800°C as a function of SiC volume fraction.

SiC clearly acts as a strong inhibitor of grain growth during the sintering of the alumina matrix. The SiC particles, highlighted in yellow, appear as small bright inclusions uniformly dispersed throughout the microstructure. At low content, they are predominantly entrapped within alumina grains, in an intragranular position (Fig. 9a). This is attributed to rapid grain growth at high temperature, which traps the fine SiC particles during grain development.

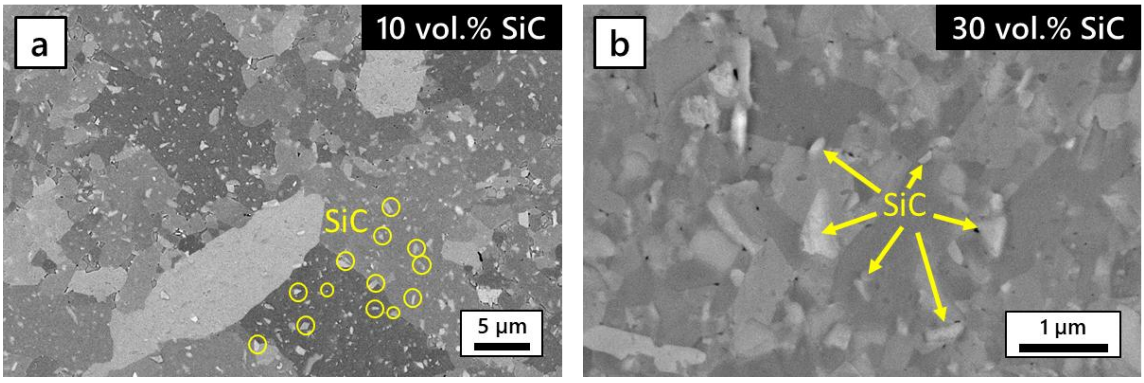

Fig. 9. High-magnification microstructures of Al_2O_3-SiC composites sintered at 1800°C with 10 and 30 vol.% SiC.

In contrast, at higher SiC contents (Fig. 9b), the localization of the SiC particles depends on their size. The finer particles remain intragranular, while coarser, angular particles, often similar in size or larger than the alumina grains, do not integrate into the matrix. These particles are instead located at grain boundaries or along the edges of alumina grains, often in close proximity but without forming true intergranular bonding.

III.2.2. Sintering optimization

To refine the microstructure and enhance the properties of the composites, sintering temperatures were adjusted for each composition, particularly for those containing less than 15 vol.% SiC, where significant grain growth was still observed. An additional objective was to suppress the formation of mullite. To achieve this, the initial sintering parameters (1800°C, no dwell time) were modified by lowering the temperature and introducing a 10 min dwell, in order to maintain sufficient densification. Furthermore, while the initial sintering experiments were performed on 30 mm diameter samples, this optimization campaign was carried out using 60 mm samples to directly match the final dimensions required for subsequent ballistic testing.

The optimal sintering temperature for pure alumina had been previously established at 1250 °C from our earlier experimental studies. However, the temperature corresponding to maximum shrinkage, determined from the displacement curves (Fig. 6), was approximately 1290°C. This indicates that the optimized temperature corresponds to roughly 97% of the maximum shrinkage temperature. This 97% rule was therefore adopted as a predictive strategy to determine the optimized sintering temperature for all compositions.

Initial sintering trials were conducted at these predicted temperatures. If the relative density achieved was below 99%, the temperature was gradually increased until the target densification was reached. The final results are presented in Fig. 10, which plots the maximum shrinkage temperature, the predicted (97%) temperature and the final optimized sintering temperature, each as a function of SiC content.

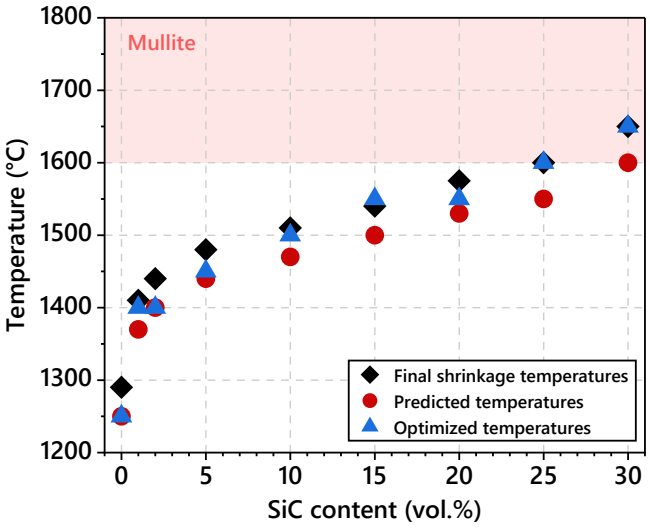

Fig. 10. Final shrinkage temperatures, predicted temperatures and optimized sintering temperatures for all Al_2O_3-SiC composite compositions.

These new sintering parameters, combining a reduced temperature with a 10 min dwell, enabled the achievement of a relative density close to 99% for all composite compositions (

Table 2).

Table 2. Relative density of Al_2O_3 and Al_2O_3-SiC composites sintered under optimized conditions as a function of SiC.

SiC content (vol.%)	0	1	2	5	10	15	20	25	30
Relative density (%)	99.2 ± 0.1	99.1 ± 0.3	98.9 ± 0.1	99.0 ± 0.2	99.0 ± 0.2	98.9 ± 0.1	98.6 ± 0.2	98.7 ± 0.2	98.6 ± 0.1

However, for the 25 and 30 vol.% SiC formulations, the temperatures required to reach full densification still fall within the range associated with mullite formation. XRD patterns obtained under these optimized conditions (Fig. 11) confirm the presence of mullite, although in significantly lower quantities compared to the initial 1800°C trials. Rietveld refinement indicated a mullite content of ~1 wt.% in the 30 vol.% SiC composite, while remaining close to the detection limit for the 25 vol.% composition.

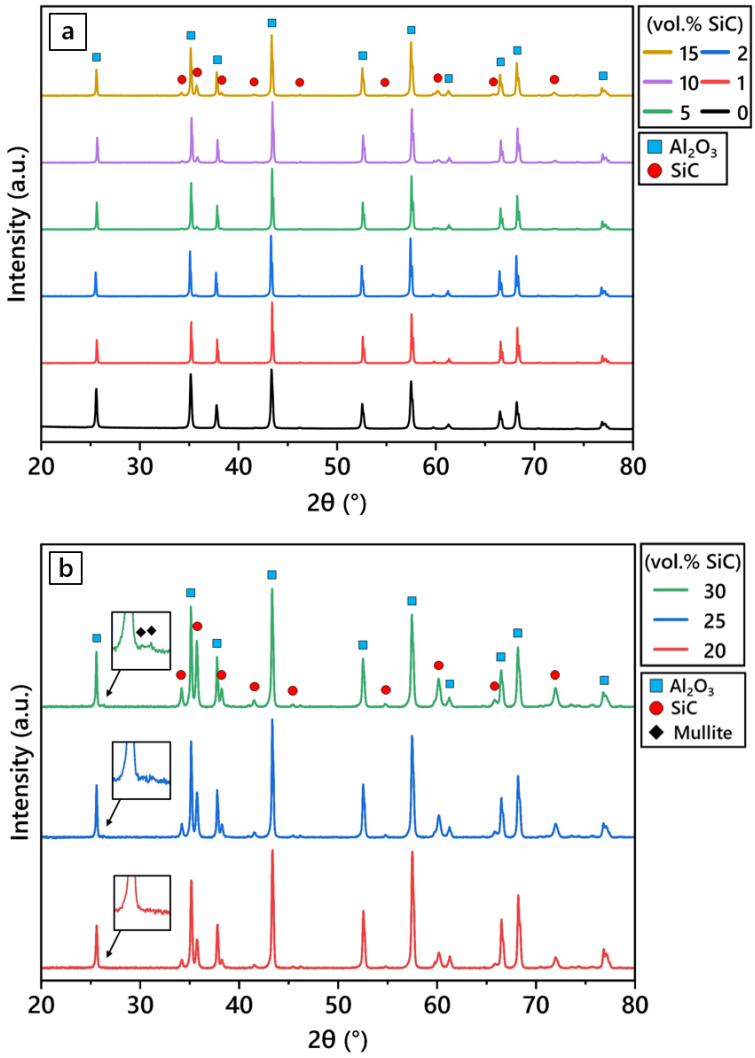

Fig. 11. XRD patterns of Al_2O_3 and Al_2O_3-SiC composites for 0-15 vol.% SiC (a) and 20-30 vol.% SiC (b).

The microstructures of the composites sintered under optimized conditions are shown in Fig. 12. For low SiC contents, the microstructure appears homogeneous, with predominantly equiaxed grains. Starting from 10 vol.% SiC, a slight morphological heterogeneity emerges, characterized by a mixture of equiaxed, elongated, and angular alumina grains. In pure alumina, the residual porosity is mainly intergranular, whereas in the composites it becomes predominantly intragranular and increases slightly with higher SiC content. This

trend correlates with the relative density measurements, as increasing SiC content leads to a gradual decrease in densification. The effect is particularly pronounced for the 20-30 vol.% SiC composites, where higher residual porosity is observed, in line with their lower relative density determined by the Archimedes method.

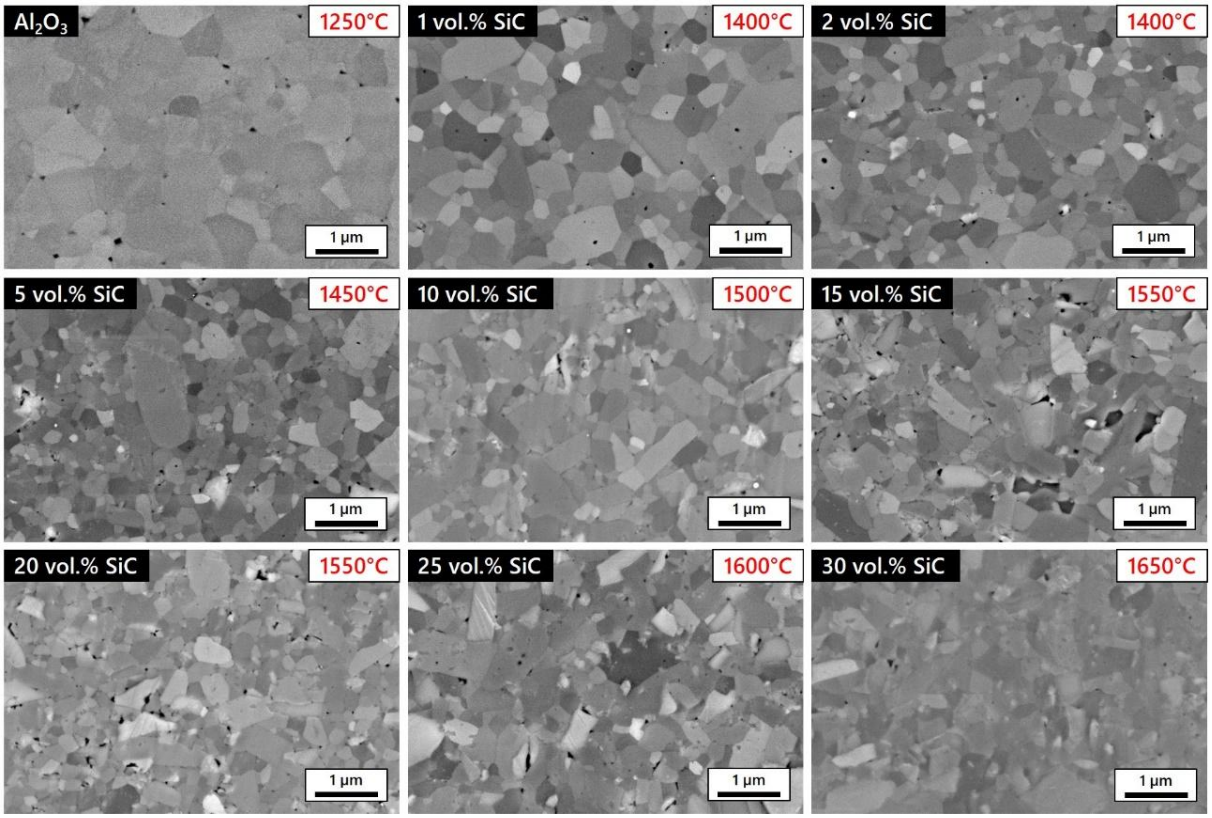

Fig. 12. Microstructures of Al_2O_3 and Al_2O_3-SiC composites sintered under optimized conditions as a function of SiC volume fraction.

Compared to the composites sintered at 1800°C, a significant reduction in grain size was observed for all compositions, particularly for SiC contents below 15 vol.%, as shown in Fig. 13. Grain size initially decreases from 0.5 µm for pure alumina to 0.23 µm with 2 vol.% SiC. Beyond this point, grain size remains relatively stable, ranging between 0.2 and 0.35 µm, despite the higher sintering temperatures required for densification.

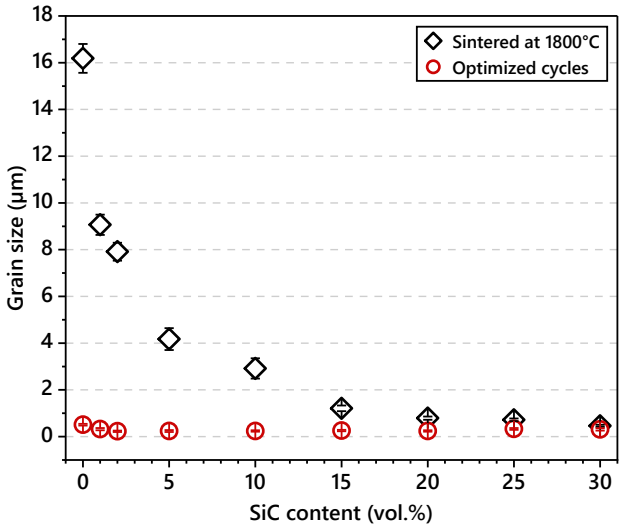

Fig. 13. Comparison of grain sizes in Al_2O_3-SiC composites sintered at 1800°C and using optimized cycles.

Comparing composites sintered under uniform conditions with those processed using optimized cycles for each composition clearly shows that the presence of SiC effectively limits grain growth in alumina. However, most studies report that this grain growth inhibition becomes more pronounced as the SiC content increases, primarily because the same sintering cycle is typically applied to all compositions [13,14,21,48]. These studies also report a decrease in relative density with increasing SiC content, as their sintering parameters are more suitable for low SiC concentrations. In contrast, when optimized sintering conditions are applied to each composition individually, the grain size remains largely consistent across the entire composition range.

III.3. Mechanical properties

The mechanical properties of the pure Al_2O_3 and Al_2O_3-SiC composites were assessed through Vickers hardness, fracture toughness, and Young's modulus measurements. To benchmark their performance, the hardness and Young's modulus values were compared with those of commercial reference ceramics.

The evolution of Vickers hardness as a function of SiC content is presented in Fig. 14. For comparison, the hardness values of composites sintered under the same conditions (1800°C) are also included in the figure. When sintered at 1800°C, a monotonic increase in hardness with increasing SiC volume fraction is observed, rising from 16.8 GPa for pure alumina to 23.3 GPa for the composite containing 30 vol.% SiC. This improvement is primarily attributed to the progressive refinement of the microstructure, consistent with the Hall-Petch effect, as well as the increasing incorporation of SiC, which is intrinsically harder than alumina [11,21]. These results are consistent with previous studies [14,23], which reported that the addition of SiC enhances the overall hardness of the composite due to its intrinsic hardness.

By optimizing the sintering temperature, the hardness of pure alumina increases markedly. It rises from 16.8 GPa when sintered at 1800°C to 22.1 GPa in the optimized cycle, which represents an improvement of approximately 31%. This improvement is explained by a substantial reduction in alumina grain size from 16 µm to 0.5 µm. A temperature of 1800°C is not at all suitable for sintering alumina. However, this beneficial effect of temperature optimization becomes progressively less pronounced as the SiC content increases. For composites containing SiC, the hardness shows only minor changes with increasing SiC fraction. After a slight initial increase at 1 and 2 vol.% SiC, it remains relatively stable and reaches 24.0 GPa at 30 vol.% SiC, which is consistent with values reported in the literature [49,50], typically ranging from 21 to 25 GPa for Al_2O_3-SiC composites. This diminished impact of optimization at higher SiC contents is consistent with the fact that the temperature difference between the standard 1800°C cycle and the optimized cycle decreases for these compositions, which limits further gains in densification and microstructural refinement. Furthermore, the overall stability in hardness across all compositions likely reflects the preservation of a similar grain size throughout the series (Fig. 13) and is less a result of the addition of SiC itself, even though SiC contributes to the composite's hardness through its own high intrinsic hardness.

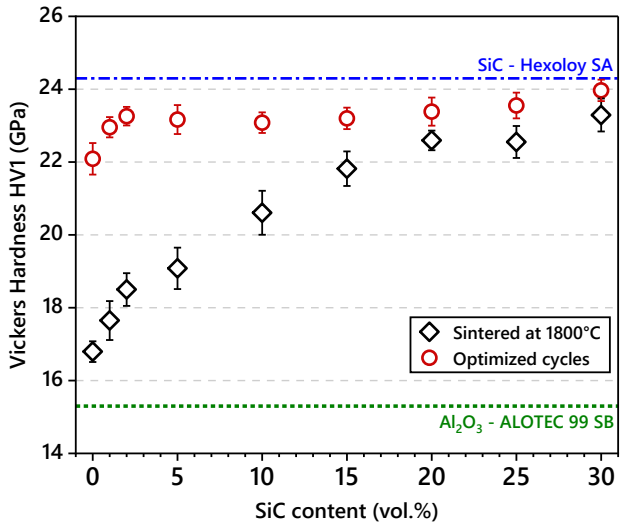

Fig. 14. Vickers hardness of pure Al_2O_3 and Al_2O_3-SiC composites as a function of SiC content, comparing samples sintered at 1800°C and with optimized cycles, along with commercial alumina and SiC references.

Although slightly lower than that of the Hexoloy SA grade, the hardness of the composites remains very similar, with the 30 vol.% SiC composite reaching 24.0 GPa compared to 24.3 GPa for Hexoloy SA SiC. These high hardness values clearly demonstrate the potential of Al_2O_3-SiC composites. In contrast, the commercial alumina reference (ALOTEC 99 SB) shows a significantly lower hardness of 15.3 GPa, underscoring the importance of microstructural optimization achieved through the tailored sintering cycles. This commercial alumina is characterized by a grain size of around 10 µm, which is much closer to the 16 µm grain size and 16.8 GPa hardness observed in the alumina sintered at 1800°C without optimization. Its lower hardness can also be partly attributed to the use of approximately 1 wt.% sintering aid during industrial processing.

Fig. 15 shows the evolution of fracture toughness as a function of SiC content. An initial decrease in fracture toughness is observed up to 2 vol.% SiC, which can be attributed to the significant increase in hardness at low SiC levels, in line with the well-known inverse relationship between hardness and fracture toughness. Beyond this threshold, a marked improvement in fracture toughness is recorded as the SiC content increases, reaching a maximum value of 4.5 $MPa.m^{1/2}$ at 25 vol.% SiC.

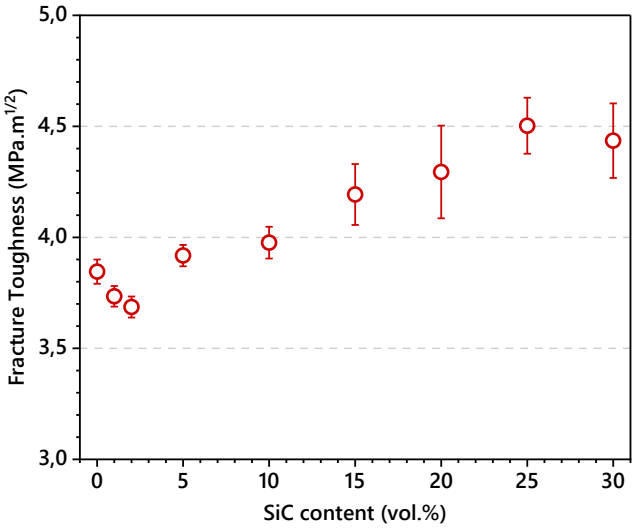

Fig. 15. Fracture toughness of pure Al_2O_3 and Al_2O_3-SiC composites sintered under optimized conditions as a function of SiC content.

This enhancement is primarily associated with extrinsic toughening mechanisms such as crack deflection and crack bridging, promoted by the presence of SiC particles. Similar observations were reported by Niihara et al. [11], who demonstrated the effectiveness of SiC particles in arresting crack propagation. In parallel, the mismatch in thermal expansion coefficients between alumina and SiC generates localized residual stresses during cooling. These stresses can activate dislocation generation and enlarge the crack-tip process zone. Acting synergistically with the crack-deflection mechanisms, these stresses contribute positively up to 25 vol.% SiC, thereby reinforcing the increase in fracture toughness.

At 30 vol.% SiC, however, the beneficial effect of residual stresses is lost. Their higher intensity promotes microcracking and reduces grain boundary cohesion, while the formation of mullite further weakens the microstructure. Together, these effects explain the slight decrease in fracture toughness observed at this composition. Additionally, the evolution of fracture toughness is also influenced by the fracture mode, as illustrated in Fig. 16, which shows the microstructural features of the fracture surfaces.

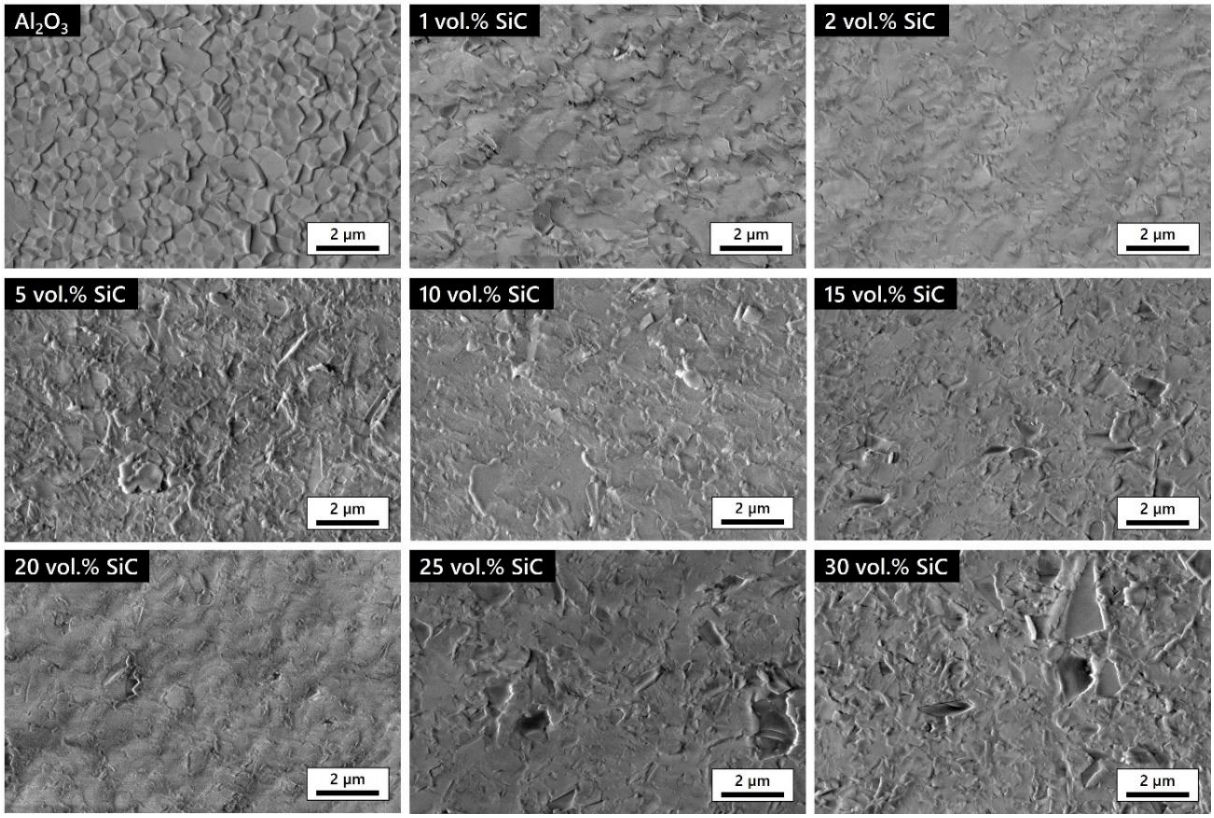

Fig. 16. Fracture surfaces of pure Al_2O_3 and Al_2O_3-SiC composites sintered under optimized conditions.

Pure alumina exhibits a predominantly intergranular fracture mode. The addition of small amounts of SiC (1 and 2 vol.%) leads to a mixed fracture mode, combining intergranular and transgranular features, which may contribute to the initial drop in fracture toughness. At higher SiC contents, the fracture becomes predominantly transgranular, promoting crack deflection through grains and a progressive increase in toughness. This transition in fracture mode, directly influenced by the microstructure induced by the presence of SiC particles, suggests that the distribution and integration of the SiC within the matrix strongly affect the energy dissipation mechanisms and, consequently, the overall mechanical behavior of the composite.

Furthermore, the observed changes in fracture behavior also highlight the importance of the good compatibility between the alumina matrix and SiC particles, as well as the effectiveness of the mixing protocol used. The apparent homogeneity of the microstructures across different compositions indicates that both precursors are

well-suited and that the mixing process ensures a uniform dispersion of SiC within the matrix, which is crucial for achieving consistent and predictable mechanical properties.

The effect of SiC addition on Young's modulus is shown in Fig. 17. The modulus remains relatively constant up to 20 vol.% SiC, with a value in the range 390-400 GPa. For higher SiC contents, an upward trend seems to be emerging, with values of 400 and 407 GPa respectively for 25 and 30 vol.% SiC. This enhancement is primarily due to the higher stiffness of SiC (450-490 GPa) compared to that of alumina (380-400 GPa). The measured values fall between those of the commercial SiC reference (423 GPa) and ALOTEC 99 alumina (372 GPa), suggesting that the stiffness behavior follows a rule of mixtures trend between the two phases.

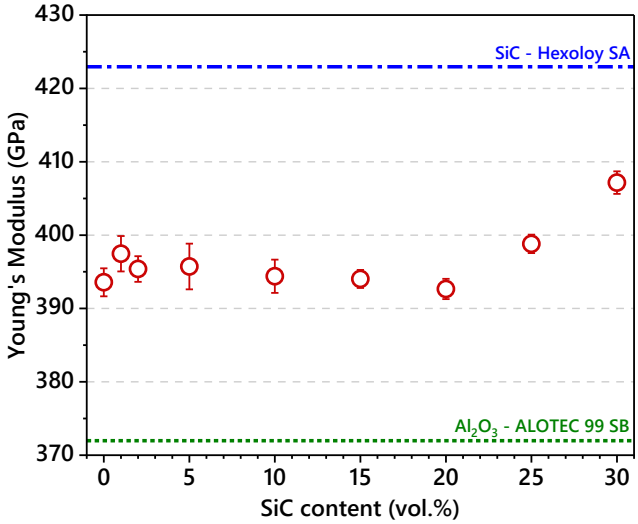

Fig. 17. Young's modulus of pure Al_2O_3 and Al_2O_3-SiC composites sintered under optimized conditions, as a function of SiC content with comparison to commercial alumina and SiC references.

Overall, the mechanical characterization of Al_2O_3-SiC composites highlights the already remarkable properties of pure alumina when sintered under optimized conditions, with significant improvements in hardness and microstructural refinement compared to conventional cycles. This high-quality baseline limits the potential gains achievable through composite design, as the hardness and Young's modulus of the composites show only modest increases with added SiC. In contrast, the most significant improvement observed with increasing SiC content lies in fracture toughness, which benefits from the transition to a more transgranular fracture mode and enhanced crack-deflection mechanisms. The optimal composition, identified around 25-30 vol.% SiC, offers a balanced enhancement in fracture toughness while maintaining high hardness and stiffness. Such a combination remains attractive for applications requiring resistance to impact, wear and crack propagation, such as ballistic protection systems.

III.4. Ballistic performance

The residual depth of penetration measured for the pure Al_2O_3 and Al_2O_3-SiC composite tiles is presented in Fig. 18, presenting individual shot values along with averages, and are compared to commercial Al_2O_3 and SiC references. Compositions containing 1 and 2 vol.% SiC were excluded from fabrication and testing because they exhibit mechanical properties similar to those of the 5 vol.% SiC composition, reducing the number of targets required.

It is important to note that some degree of scatter is observed in the DOP results. This variability is normal for brittle materials under ballistic impact and is also seen in industrially produced reference ceramics. While commercial SiC tends to be highly reproducible, some variability still exists. This dispersion can be attributed

to variations in target properties (such as microstructure and density), projectile characteristics (including mass, velocity, material and shape), and experimental conditions (such as surface finish, impact angle, target thickness, mounting method and environmental factors).

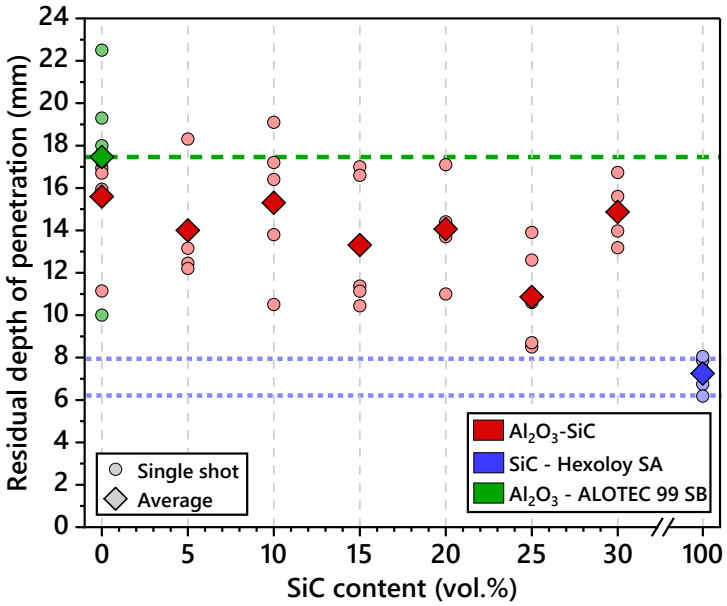

Fig. 18. Residual depth of penetration in pure Al_2O_3 and Al_2O_3-SiC composites compared to commercial alumina and SiC references as a function of SiC content.

The ballistic characterization begins with the assessment of pure alumina, which already shows improved performance compared to the commercial alumina reference (ALOTEC 99 SB). The average residual depth of penetration decreases from 17.5 mm for ALOTEC to 15.6 mm for pure alumina, corresponding to an improvement of approximately 11%. However, despite this enhancement, pure alumina remains significantly less effective than the commercial SiC reference, which achieves an average residual DOP of 7.25 mm.

When introducing SiC into the alumina matrix, the overall trend shows a reduction in residual DOP up to 25 vol.% SiC, after which the performance slightly declines at 30 vol.% SiC. The 25 vol.% SiC composite achieves the best performance among the tested compositions, with an average residual DOP of 10.9 mm (Fig. 19). This corresponds to a reduction of approximately 30% compared to pure alumina, and it represents a narrowing of the gap with commercial SiC, offering a promising intermediate solution at lower cost.

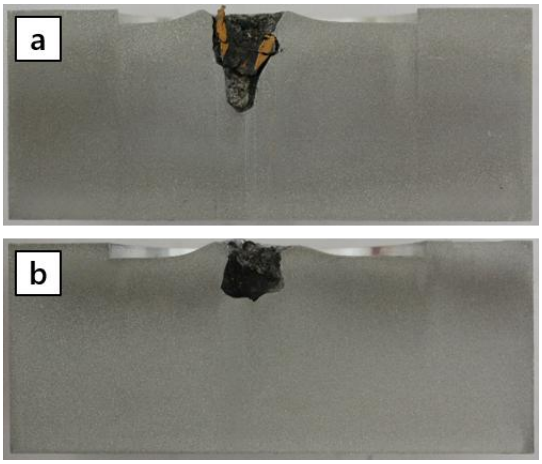

Fig. 19. Residual depth of penetration for pure Al_2O_3 (a) and Al_2O_3-SiC composite with 25 vol.% SiC (b).

It should be noted that while the general trend is one of decreasing DOP with increasing SiC content, the variation is not perfectly linear. The drop in DOP is particularly clear when excluding the 30 vol.% SiC composition, where the presence of mullite and the possible amplification of residual stresses are assumed to negatively affect fracture toughness and grain boundary cohesion. These factors likely contribute to the slight rebound in penetration depth observed at this composition. This indicates that the 25 vol.% SiC composition stands out as the optimal formulation, even though its superior performance is not fully predicted by a simple monotonic trend with SiC content.

The improvement in ballistic performance can primarily be attributed to the increase in fracture toughness with SiC addition, while other mechanical properties such as hardness and Young's modulus show more limited changes. The higher toughness promotes more effective crack deflection and energy dissipation upon impact, which is crucial given the very thin target thicknesses tested here (around 2.3 mm for pure alumina, increasing slightly to 2.42 mm for the 25 vol.% SiC composite). This small increase in thickness, enabled by the lower density of SiC while maintaining constant areal density, also contributes modestly to performance [7].

These observations are consistent with results in the literature, such as those reported by Azarafza et al. [30], who demonstrated through numerical simulations that adding 10 vol.% SiC significantly improves the ballistic resistance of alumina-based materials due to enhanced fracture toughness and flexural strength. As expected, the commercial SiC reference remains superior overall, with residual penetration depths ranging from 6.2 to 8.0 mm. Nonetheless, the best-performing composite with 25 vol.% SiC achieves approximately 8.6 mm residual penetration, a relatively small difference that underscores the potential of Al_2O_3-SiC composites as a cost-effective alternative for ballistic protection systems.

These findings underline the value of performing multiple tests to obtain robust assessments of ballistic performance, particularly given the inherent variability of brittle materials. Further experimental work with additional samples would help strengthen the statistical reliability of these results and deepen the understanding of the relationships among processing parameters, microstructure, mechanical properties and ballistic behavior. In parallel, advanced characterizations, such as residual stress measurements by diffraction or high-resolution TEM analyses of crack-particle interactions, would provide deeper insight into the micromechanical mechanisms responsible for the observed ballistic performance.

In conclusion, the Al_2O_3-SiC composites developed in this study, and especially the 25 vol.% SiC composition, offer a promising balance between cost and performance, demonstrating their potential as effective solutions for lightweight ballistic protection applications.

CONCLUSION

This study aimed to develop cost-effective Al_2O_3-SiC composites with improved ballistic performance through controlled processing. Using planetary ball milling and optimized SPS cycles tailored for each composition, high-density materials with refined microstructures were achieved while minimizing unwanted phases like mullite.

For pure alumina, the optimized cycle delivered remarkable improvements, reducing grain size from 16 µm to about 0.5 µm and increasing hardness by 31% (from 16.8 GPa to 22.1 GPa), clearly outperforming commercial alumina (ALOTEC 99 SB). Adding SiC further inhibited grain growth and primarily enhanced fracture toughness, which peaked at 4.5 $MPa \cdot m^{1/2}$ for the 25 vol.% SiC composite, due to effective crack deflection and bridging. Hardness and Young's modulus increased more modestly.

A small amount of mullite was detected at higher SiC contents, slightly lowering mechanical and ballistic performance at 30 vol.% SiC. Ballistic tests on thin tiles confirmed the benefit of SiC addition: the 25 vol.% composite reduced residual DOP by 30 % compared to pure alumina (from 15.6 mm to 10.9 mm), approaching the performance of commercial SiC (7.25 mm).

Although some variability was observed, typical of thin brittle targets, these results demonstrate the potential of Al_2O_3-SiC composites, especially at 25 vol.% SiC, as promising, cost-effective solutions for lightweight ballistic protection. Further tests with more samples would help confirm and refine these promising trends.

ACKNOWLEDGEMENTS

This research is funded by Direction Générale pour l'Armement (DGA) through a PhD grant and by the French National Agency for Research under grant agreement n° ANR-22-ASTR-0001. (MOCA project). The authors acknowledge the assistance of Thierry Bourré and Julie Rossit from ISL for samples preparation.

REFERENCES

[1] P.J. Hazell, Armour: Materials, Theory, and Design, 2nd ed., CRC Press, Boca Raton, 2022. https://doi.org/10.1201/9781003322719.

[2] M.S. Boldin, N.N. Berendeev, N.V. Melekhin, A.A. Popov, A.V. Nokhrin, V.N. Chuvildeev, Review of ballistic performance of alumina: Comparison of alumina with silicon carbide and boron carbide, Ceram. Int. 47 (2021) 25201–25213. https://doi.org/10.1016/j.ceramint.2021.06.066.

[3] P.H.P.M. da Silveira, T.T. da Silva, M.P. Ribeiro, P.R. Rodrigues de Jesus, P.C.R. dos S. Credmann, A.V. Gomes, A Brief Review of Alumina, Silicon Carbide and Boron Carbide Ceramic Materials for Ballistic Applications, Acad. Lett. (2021). https://doi.org/10.20935/AL3742.

[4] N.D. Andraskar, G. Tiwari, M.D. Goel, Impact response of ceramic structures - A review, Ceram. Int. 48 (2022) 27262–27279. https://doi.org/10.1016/j.ceramint.2022.06.313.

[5] I.G. Crouch, The science of armour materials, 1st edition, Elsevier, Waltham, MA, 2016.

[6] S.G. Savio, D.A. Babu, B. Ramakrishna, S. Singh, C. Vanitha, Influence of sintering process on microstructure and mechanical properties of alumina ceramics: Spark plasma and microwave hybrid sintering, Ceram. Int. 50 (2024) 11730–11742. https://doi.org/10.1016/j.ceramint.2024.01.078.

[7] A.B. Dresch, J. Venturini, S. Arcaro, O.R.K. Montedo, C.P. Bergmann, Ballistic ceramics and analysis of their mechanical properties for armour applications: A review, Ceram. Int. 47 (2021) 8743–8761. https://doi.org/10.1016/j.ceramint.2020.12.095.

[8] R. Yadav, M. Naebe, X. Wang, B. Kandasubramanian, Body armour materials: from steel to contemporary biomimetic systems, RSC Adv. 6 (2016) 115145–115174. https://doi.org/10.1039/C6RA24016J.

[9] U. Salma, M. Hasanuzzaman, I.U. Bhuiyan, S. Hashmi, High strength alumina composite for protective armors: A review, in: Compr. Mater. Process., Elsevier, 2024: pp. 67–78. https://doi.org/10.1016/B978-0-323-96020-5.00001-7.

[10] A. Ruys, Alumina in lightweight body armor, in: Alumina Ceram., Elsevier, 2019: pp. 321–368. https://doi.org/10.1016/B978-0-08-102442-3.00011-7.

[11] K. Niihara, New Design Concept of Structural Ceramics: Ceramic Nanocomposites, J. Ceram. Soc. Jpn. 99 (1991) 974–982. https://doi.org/10.2109/jcersj.99.974.

[12] J. Zhao, L.C. Stearns, M.P. Harmer, H.M. Chan, G.A. Miller, R.F. Cook, Mechanical Behavior of Alumina-Silicon Carbide "Nanocomposites," J. Am. Ceram. Soc. 76 (1993) 503–510. https://doi.org/10.1111/j.1151-2916.1993.tb03814.x.

[13] Y.L. Dong, F.M. Xu, X.L. Shi, C. Zhang, Z.J. Zhang, J.M. Yang, Y. Tan, Fabrication and mechanical properties of nano-/micro-sized Al2O3/SiC composites, Mater. Sci. Eng. A 504 (2009) 49–54. https://doi.org/10.1016/j.msea.2008.10.021.

[14] M. Parchovianský, D. Galusek, J. Sedláček, P. Švančárek, M. Kašiarová, J. Dusza, P. Šajgalík, Microstructure and mechanical properties of hot pressed Al2O3/SiC nanocomposites, J. Eur. Ceram. Soc. 33 (2013) 2291–2298. https://doi.org/10.1016/j.jeurceramsoc.2013.01.024.

[15] Z. Rosenberg, E. Dekel, Terminal Ballistics, Springer Berlin Heidelberg, Berlin, Heidelberg, 2012. https://doi.org/10.1007/978-3-642-25305-8.

[16] C.E. Borsa, S. Jiao, R.I. Todd, R.J. Brook, Processing and properties of Al2O3/SiC nanocomposites, J. Microsc. 177 (1995) 305–312. https://doi.org/10.1111/j.1365-2818.1995.tb03561.x.

[17] D. Sciti, J. Vicens, A. Bellosi, Microstructure and properties of alumina-SiC nanocomposites prepared from ultrafine powders, J. Mater. Sci. 37 (2002) 3747–3758. https://doi.org/10.1023/A:1016577728915.

[18] E. Akbari, M. Ghassemi Kakroudi, V. Shahedifar, H. Ghiasi, The influence of different SiC amounts on the microstructure, densification, and mechanical properties of hot-pressed Al 2 O 3 -SiC composites, Int. J. Appl. Ceram. Technol. 17 (2020) 491–500. https://doi.org/10.1111/ijac.13406.

[19] I. Álvarez, R. Torrecillas, W. Solis, P. Peretyagin, A. Fernández, Microstructural design of Al2O3–SiC nanocomposites by Spark Plasma Sintering, Ceram. Int. 42 (2016) 17248–17253. https://doi.org/10.1016/j.ceramint.2016.08.019.

[20] H.Z. Wu, C.W. Lawrence, S.G. Roberts, B. Derby, The strength of Al2O3/SiC nanocomposites after grinding and annealing, Acta Mater. 46 (1998) 3839–3848. https://doi.org/10.1016/S1359-6454(98)00068-8.

[21] J. Chai, Y. Zhu, X. Gao, T. Shen, L. Niu, S. Li, P. Jin, M. Cui, Z. Wang, Effects of residual stress and intragranular particles on mechanical properties of hot-pressed Al2O3/SiC ceramic composites, Ceram. Int. 48 (2022) 23258–23265. https://doi.org/10.1016/j.ceramint.2022.04.310.

[22] I. Levin, W.D. Kaplan, D.G. Brandon, T. Wieder, Residual stresses in alumina-SiC nanocomposites, Acta Metall. Mater. 42 (1994) 1147–1154. https://doi.org/10.1016/0956-7151(94)90131-7.
[23] X. Sun, J.-G. Li, S. Guo, Z. Xiu, K. Duan, X.Z. Hu, Intragranular Particle Residual Stress Strengthening of Al2O3-SiC Nanocomposites, J. Am. Ceram. Soc. 88 (2005) 1536–1543. https://doi.org/10.1111/j.1551-2916.2005.00309.x.
[24] Y. Luo, Y. Wu, D. Xiao, K. Tang, C. Huang, R.K.Y. Fu, S. Zheng, P.K. Chu, Al2O3 coating for densification of SiC ceramics and sintering kinetics, Surf. Coat. Technol. 374 (2019) 603–609. https://doi.org/10.1016/j.surfcoat.2019.06.040.
[25] L.P. Ferroni, G. Pezzotti, Evidence for Bulk Residual Stress Strengthening in Al2O3/SiC Nanocomposites, J. Am. Ceram. Soc. 85 (2002) 2033–2038. https://doi.org/10.1111/j.1151-2916.2002.tb00400.x.
[26] S.-M. Choi, H. Awaji, Nanocomposites—a new material design concept, Sci. Technol. Adv. Mater. 6 (2005) 2–10. https://doi.org/10.1016/j.stam.2004.06.002.
[27] T. Ohji, Y.-K. Jeong, Y.-H. Choa, K. Niihara, Strengthening and Toughening Mechanisms of Ceramic Nanocomposites, J. Am. Ceram. Soc. 81 (2005) 1453–1460. https://doi.org/10.1111/j.1151-2916.1998.tb02503.x.
[28] S. Jiao, M.L. Jenkins, R.W. Davidge, Interfacial fracture energy-mechanical behaviour relationship in Al2O3/SiC and Al2O3/TiN nanocomposites, Acta Mater. 45 (1997) 149–156. https://doi.org/10.1016/S1359-6454(96)00168-1.
[29] L. Gao, H.Z. Wang, J.S. Hong, H. Miyamoto, K. Miyamoto, Y. Nishikawa, Mechanical Properties and Microstructure of Nano-SiC/Al2O3 Composites Densified by Spark Plasma Sintering, (1998).
[30] R. Azarafza, Impact Behavior of Ceramic- Metal Armour Composed of Al2O3-Nano SiC Composite, Int. J. Adv. Des. Manuf. Technol. 5 (2012) 83–87.
[31] S. Jamale, A. Kumar, M.A. Iqbal, B.V. Manoj Kumar, Ballistic resistance of spark plasma sintered B4C-SiC composites, Ceram. Int. 51 (2025) 27088–27097. https://doi.org/10.1016/j.ceramint.2025.03.340.
[32] M. Razavi, A.R. Farajipour, M. Zakeri, M.R. Rahimipour, A.R. Firouzbakht, Production of Al2O3–SiC nano-composites by spark plasma sintering, Bol. Soc. Esp. Cerámica Vidr. 56 (2017) 186–194. https://doi.org/10.1016/j.bsecv.2017.01.002.
[33] A. Borrell, I. Álvarez, R. Torrecillas, V.G. Rocha, A. Fernández, Microstructural design for mechanical and electrical properties of spark plasma sintered Al2O3–SiC nanocomposites, Mater. Sci. Eng. A 534 (2012) 693–698. https://doi.org/10.1016/j.msea.2011.12.032.
[34] J.H. Chae, K.H. Kim, Y.H. Choa, J. Matsushita, J.-W. Yoon, K.B. Shim, Microstructural evolution of Al2O3–SiC nanocomposites during spark plasma sintering, J. Alloys Compd. 413 (2006) 259–264. https://doi.org/10.1016/j.jallcom.2005.05.049.
[35] O.T. Johnson, P. Rokebrand, I. Sigalas, Microstructure and Properties of Al2O3–SiC Nanomaterials, Proc. World Congr. Eng. 2 (2014).
[36] H.-E. Kim, A.J. Moorhead, S.-H. Kim, Strengthening of Alumina by Formation of a Mullite/Glass Layer on the Surface, J. Am. Ceram. Soc. 80 (1997) 1877–1880. https://doi.org/10.1111/j.1151-2916.1997.tb03064.x.
[37] V. Garnier, G. Fantozzi, D. Nguyen, J. Dubois, G. Thollet, Influence of SiC whisker morphology and nature of SiC/Al2O3 interface on thermomechanical properties of SiC reinforced Al2O3 composites, J. Eur. Ceram. Soc. 25 (2005) 3485–3493. https://doi.org/10.1016/j.jeurceramsoc.2004.09.026.
[38] Makri Hocine, Elaboration d'un composite multiphases zircon-alumine-mullite-zircone, PhD thesis, University of Ferhat Abbas-Setif Ufas, 2015.
[39] ASTM E112-13, Standard Test Methods for Determining Average Grain Size, ASTM International, 2013.
[40] ASTM C1327-08, Standard Test Method for Vickers Indentation Hardness of Advanced Ceramics, ASTM International, 2008.
[41] K. Niihara, R. Morena, D.P.H. Hasselman, Evaluation of KIc of brittle solids by the indentation method with low crack-to-indent ratios, J. Mater. Sci. Lett. 1 (1982) 13–16. https://doi.org/10.1007/BF00724706.
[42] L.-S. Chang, T.-H. Chuang, W.J. Wei, Characterization of alumina ceramics by ultrasonic testing, Mater. Charact. 45 (2000) 221–226. https://doi.org/10.1016/S1044-5803(00)00081-4.
[43] VPAM APR. Vereinigung der Prüfstellen für angriffshemmende materialien und konstruktionen general basis for ballistic material, construction and product tests requirements, test levels and test procedures, VPAM APR Ed., 2021.

[44] R. Klement, P. Švančárek, M. Parchovianský, J. Sedláček, D. Galusek, Al2O3 -SiC nanocomposites, in: Adv. Ceram. Matrix Compos., Elsevier, 2018: pp. 49–92. https://doi.org/10.1016/B978-0-08-102166-8.00004-9.
[45] J. Pérez-Rigueiro, J.Y. Pastor, J. Llorca, M. Elices, P. Miranzo, J.S. Moya, Revisiting the mechanical behavior of alumina/silicon carbide nanocomposites, Acta Mater. 46 (1998) 5399–5411. https://doi.org/10.1016/S1359-6454(98)00193-1.
[46] M. Sternitzke, Structural ceramic nanocomposites, J. Eur. Ceram. Soc. 17 (1997) 1061–1082. https://doi.org/10.1016/S0955-2219(96)00222-1.
[47] Z.-Y. Deng, J.-L. Shi, Y.-F. Zhang, D.-Y. Jiang, J.-K. Guo, Pinning effect of SiC particles on mechanical properties of Al2O3–SiC ceramic matrix composites, J. Eur. Ceram. Soc. 18 (1998) 501–508. https://doi.org/10.1016/S0955-2219(97)00164-7.
[48] S. Ghadami, H. Baharvandi, F. Ghadami, Influence of the vol% SiC on properties of pressureless Al2O3/SiC nanocomposites, J. Compos. Mater. 50 (2016) 1367–1375. https://doi.org/10.1177/0021998315591300.
[49] X.L. Shi, F.M. Xu, Z.J. Zhang, Y.L. Dong, Y. Tan, L. Wang, J.M. Yang, Mechanical properties of hot-pressed Al2O3/SiC composites, Mater. Sci. Eng. A 527 (2010) 4646–4649. https://doi.org/10.1016/j.msea.2010.03.035.
[50] A. Moradkhani, H. Baharvandi, A. Naserifar, Effect of Sintering Temperature on the Grain Size and Mechanical Properties of Al2O3-SiC Nanocomposites, J. Korean Ceram. Soc. 56 (2019) 256–268. https://doi.org/10.4191/kcers.2019.56.3.01.